

---

# Oracle Supervision Transfers for Hyperparameter Prediction in Model-Based Image Denoising

---

**Jianmin Liao\***

Department of Mathematics  
Syracuse University  
jliao21@syr.edu

**Lixin Shen**

Department of Mathematics  
Syracuse University  
lshen03@syr.edu

**Yuesheng Xu**

Department of Mathematics & Statistics  
Old Dominion University  
y1xu@odu.edu

## Abstract

Hyperparameter prediction is a critical practical bottleneck for model-based image denoisers, ranging from classical TV/TGV variational solvers to modern diffusion-based models such as DiffPIR. While existing learned predictors can achieve near-oracle performance, this approach scales poorly: each new configuration conventionally requires its own oracle-labeled training set, and each label requires a hierarchical grid search evaluated against clean ground truth. We therefore ask whether oracle supervision collected on source configurations can transfer to target configurations with few or no target oracle labels. We propose HyperDn, a single configuration-conditioned predictor that pools oracle supervision across source configurations and predicts heterogeneous hyperparameters for new denoiser-noise configurations. In a cross-paradigm experiment, HyperDn transfers from relatively cheap TV/TGV variational sources to more expensive diffusion-based DiffPIR. With only 2 target oracle labels, it reaches 30.23 dB, within 0.90 dB of the oracle, and outperforms the 64-label per-configuration predictor trained from scratch, using  $1/32$  as many target labels as that baseline point. Without any target oracle labels, HyperDn also reaches near-oracle PSNR on two unseen mixtures of seen noise types and on transfer from relatively cheap  $96 \times 96$  source images to  $512 \times 768$  targets. Together, these results show that expensive oracle supervision for hyperparameter prediction can be transferred from source to new target configurations, reducing the need to rebuild oracle labels for each new denoising configuration.

## 1 Introduction

Model-based image denoisers remain widely used and continue to evolve, from classical TV [Rudin et al., 1992] and total generalized variation (TGV) [Bredies et al., 2010] variational solvers to recent diffusion-based denoisers such as DiffPIR [Zhu et al., 2023]. Using these methods typically requires hyperparameter selection: choosing values that maximize reconstruction quality (e.g., PSNR) for a given degraded image and denoiser-noise *configuration*, where a configuration is the denoiser together with the noise type. This selection is important because hyperparameters strongly affect reconstruction quality. It is also difficult because selecting such values amounts to specifying a map from images and configurations to hyperparameters, which is hard to design by hand. Learned

---

\*Corresponding author.

predictors such as Afkham et al. [2021] use deep neural networks to predict regularization parameters for inverse problems. With sufficient data for a fixed configuration, they produce hyperparameters with near-oracle reconstruction quality.

However, this oracle supervision is expensive. Building labels for one configuration is heavy: each denoiser call is slow (e.g.,  $\approx 10$  s for DiffPIR on a  $256 \times 256$  image), each training image requires running the denoiser with many candidate hyperparameters and evaluating each output against the ground truth image, and this is repeated for every training image. The number of configurations,  $N_{\text{cfg}}$ , is also large because each is a combination of a denoiser and a noise type, and both axes are wide. There are numerous existing denoisers, including but not limited to variational and diffusion-based ones. Noise types include Gaussian, Poisson, black-and-white impulse, RGB impulse, and their mixtures. Both axes keep expanding as new methods and new noise mixtures appear. The total cost therefore scales as

$$\underbrace{t_{\text{call}}}_{\text{sec/call}} \times \underbrace{K_{\text{sweep}}}_{\text{candidates/image}} \times \underbrace{N_{\text{img}}}_{\text{training images}} \times \underbrace{N_{\text{cfg}}}_{\text{configurations}} .$$

We raise the question: can supervision for predicting hyperparameters transfer across configurations to substantially reduce the oracle label need for new configurations? Two observations make this plausible. First, across denoisers, the optimal hyperparameter setting depends on similar properties of the input image, such as noise types and strength, texture, and edges. Second, the hyperparameters of many model-based denoisers have similar roles across methods, even if not identical. For instance, TV, TGV, and DiffPIR all fit  $\hat{x} = \arg \min_{\mathbf{u}} D(\mathbf{u}, \mathbf{y}) + \lambda R(\mathbf{u})$ , where  $\lambda$  in each method is a trade-off weight between data fidelity and the prior. Knowledge learned on relatively cheap TV and TGV configurations could therefore partially transfer to the more expensive DiffPIR.

We answer this question with HyperDn, a single predictor trained on oracle labels pooled across 13 source configurations and transferred to new ones. It takes a degraded image, a configuration identifier, and optional metadata, and outputs the queried configuration’s hyperparameters. A shared image encoder extracts the input-image properties common across configurations. A configuration-conditioned output head addresses two output-space challenges: different numbers of hyperparameters, and shared hyperparameters such as  $\lambda$  that have similar but not identical semantics.

Three experiments show that oracle hyperparameter supervision transfers across denoising paradigms, noise mixtures, and image resolutions. First, HyperDn transfers from relatively cheap TV/TGV sources to more expensive DiffPIR with just 2 target labels, coming within 0.9 dB of the oracle and outperforming the 64-label per-configuration predictor trained from scratch. This uses 1/32 as many target labels as that baseline point. Second, with zero target labels, it predicts hyperparameters for noise mixtures whose types were seen separately during training. Third, also with zero target labels, it transfers from relatively cheap  $96 \times 96$  training images to  $512 \times 768$  test images, where each oracle label costs roughly  $40 \times$  more denoiser time.

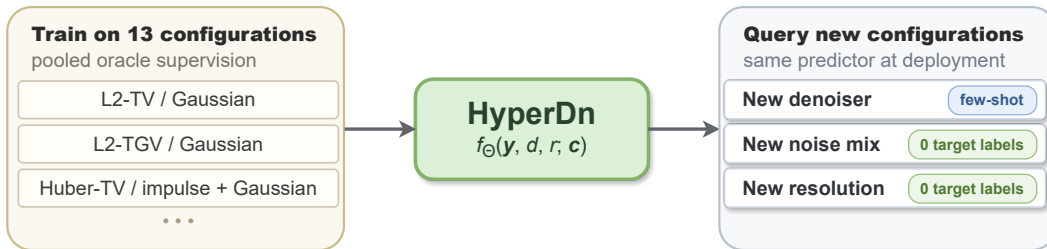


Figure 1: **HyperDn: one predictor, many configurations.** A single conditional predictor  $f_{\Theta}(\mathbf{y}, d, r; \mathbf{c})$ , where  $\mathbf{y}$  is the degraded image,  $d, r$  are identifiers of the queried denoiser, and  $\mathbf{c}$  is an optional encoding of noise attributes and observation metadata, is trained on pooled oracle supervision. The same predictor is adapted with few target labels to a new denoiser (DiffPIR) and applied zero-shot to new mixtures of noise types seen separately during training and to larger target resolutions.

**Contributions.**

- **Oracle hyperparameter labels as transferable supervision.** We propose that oracle hyperparameter labels can transfer across denoising configurations, rather than serving only the single configuration they were built for.
- **Pooled multi-configuration training.** HyperDn trains a single predictor on oracle labels pooled from 13 source configurations; a shared image encoder captures input-image properties and a configuration-conditioned output head handles configuration-specific hyperparameters.
- **Transfer in cost-asymmetric directions.** HyperDn transfers from configurations with relatively cheap oracle labels (relatively fast TV/TGV variational solves; small source images) to configurations with more expensive oracle labels (DiffPIR diffusion sampling; high-resolution test images). With only 2 DiffPIR target labels, it comes within 0.9 dB of the DiffPIR oracle and outperforms the 64-label per-configuration predictor trained from scratch, using 1/32 as many target labels as that baseline point. Without any target labels, it stays within  $\sim 0.2$  dB of oracle on novel noise mixtures and transfers from  $96 \times 96$  source images to  $512 \times 768$  targets, where each oracle label costs roughly  $40\times$  more denoiser time.

## 2 HyperDn

Given a degraded image and a denoising configuration, HyperDn predicts the hyperparameters needed to reconstruct that image. We represent configuration-specific hyperparameters in a padded vector (Figure 2). A single configuration-conditioned predictor then shares information across configurations while preserving each denoiser’s numerical range. It is trained on oracle labels pooled across the source configurations.

### 2.1 Problem Setting: Oracle-Supervised Hyperparameter Prediction

We formalize oracle-supervised hyperparameter prediction by defining the hyperparameter vector  $\mathbf{p}$ , the training and test data, and HyperDn’s input/output.

**Configuration and hyperparameter vector.** We consider model-based denoisers whose objective decomposes into a data term  $D$  and a prior term  $R$ . In our experiments,  $D$  ranges over L2, Huber, and negative-log-likelihood-style (NLL) data terms for Poisson or Poisson–Gaussian observations;  $R$  ranges over TV, TGV, and DiffPIR; observation noise spans Gaussian, Poisson, Poisson–Gaussian, impulse, and mixtures thereof. A denoising configuration is defined as a tuple  $(d, r; \mathbf{c})$ , where  $d$  is the data-term identifier,  $r$  is the prior-term identifier, and  $\mathbf{c}$  encodes any available noise attributes and observation metadata (empty when none are provided).

For each configuration, the hyperparameter vector is a padded vector  $\mathbf{p} \in \mathbb{R}^{L_{\max}}$ , where  $L_{\max}$  is the maximum hyperparameter-vector length among the supported configurations. The pair  $(d, r)$  determines which coordinates of  $\mathbf{p}$  are active hyperparameters and which are padding. The Huber data term has one hyperparameter, the threshold  $\delta$ ; L2 and NLL have none. TV and DiffPIR have the prior weight  $\lambda$ ; TGV has  $\lambda$  together with the second-order to first-order weight ratio  $\gamma$ . We write  $\mathbf{p} = (p_\delta, p_\lambda, p_\gamma)$ . Entries for hyperparameters not used by  $(d, r)$  are set to a fixed padding value.

**Training and test data.** The dataset consists of tuples  $(\mathbf{y}, \mathbf{x}, d, r, \mathbf{c})$ , where  $\mathbf{x}$  is the clean image; each tuple is paired with an oracle hyperparameter target  $\mathbf{p}^*$ . Let  $\mathcal{R}_{d,r}(\mathbf{y}; \mathbf{p})$  denote the denoiser output for  $\mathbf{y}$  under configuration  $(d, r)$  with hyperparameters  $\mathbf{p}$ ,  $\mathcal{P}(d, r)$  the set of candidate hyperparameter vectors for  $(d, r)$ , and  $Q$  a quality criterion to be maximized (PSNR in our experiments). Other quality criteria (e.g., structural or perceptual metrics) would yield different oracle labels. We use PSNR throughout, so all transfer results share the same target. The oracle target maximizes  $Q$  against the clean image:

$$\mathbf{p}^* \in \arg \max_{\mathbf{p} \in \mathcal{P}(d,r)} Q(\mathcal{R}_{d,r}(\mathbf{y}; \mathbf{p}), \mathbf{x}). \quad (1)$$

At test time,  $\mathbf{x}$  is unavailable, so the oracle cannot be evaluated; the test set thus consists of tuples  $(\mathbf{y}, d, r, \mathbf{c})$  without  $\mathbf{x}$ .

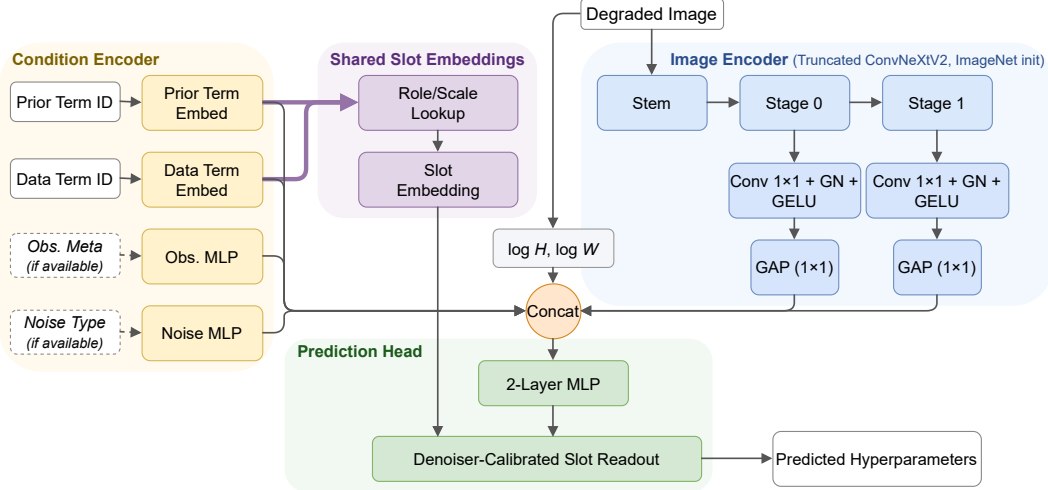


Figure 2: HyperDn architecture. A shared image encoder built on a truncated ConvNeXtV2 (stem and stages 0–1, ImageNet-pretrained) extracts features from the degraded image. A configuration-conditioned output head, comprising a condition encoder, shared slot embeddings, and a denoiser-calibrated slot readout, produces the padded hyperparameter vector for the queried configuration; padding slots are ignored in the loss.

**Predictor input/output.** HyperDn is a learned predictor  $f_{\Theta}$  with parameters  $\Theta$ . Given configuration  $(d, r; c)$  and degraded image  $\mathbf{y}$ ,  $f_{\Theta}$  produces a padded hyperparameter vector

$$\hat{\mathbf{p}} = f_{\Theta}(\mathbf{y}, d, r; c) \in \mathbb{R}^{L_{\max}}, \quad (2)$$

in the same padded format as the oracle target  $\mathbf{p}^*$ . The parameters  $\Theta$  are learned from the training set. At test time,  $\hat{\mathbf{p}}$  is plugged into the denoiser to produce the reconstruction  $\mathcal{R}_{d,r}(\mathbf{y}; \hat{\mathbf{p}})$ .

## 2.2 Architecture: Configuration-Conditioned Hyperparameter Prediction

HyperDn has two parts: a shared encoder and an output head. The encoder uses one set of weights for all configurations, producing a feature  $\mathbf{h}$  from the image and configuration  $(d, r; c)$ . The output head is designed to share hyperparameter roles across configurations while still distinguishing how each denoiser uses those roles. For example,  $\lambda$  plays a prior-weight role—the weight balancing the prior against data fidelity—in TV, TGV, and DiffPIR, so supervision from one denoiser helps the predictor learn how to choose  $\lambda$  from the image in another. But these  $\lambda$  values are not numerically interchangeable: each denoiser uses its prior weight in its own numerical range. Configurations also activate different sets of hyperparameters (e.g., L2-TV activates only  $\lambda$ , while Huber-TGV activates  $\delta$ ,  $\lambda$ , and  $\gamma$ ), and the head must predict each configuration’s active set. HyperDn therefore represents the output as padded *slots*: each coordinate of  $\mathbf{p}$  is called a slot, and under  $(d, r)$  a slot is either active (it holds a hyperparameter) or padding. The output head is a denoiser-calibrated slot readout that maps  $\mathbf{h}$  plus per-slot metadata to  $\hat{\mathbf{p}}$ . Figure 2 shows the architecture of HyperDn.

**Image and configuration encoder.** The image encoder uses an ImageNet-pretrained [Deng et al., 2009] ConvNeXtV2 [Woo et al., 2023] truncated to its stem and stages 0–1. For each retained stage, a  $1 \times 1$  convolution projects the spatial features to a fixed channel dimension, followed by global average pooling to produce a per-stage vector. These per-stage vectors are concatenated with  $\log H$  and  $\log W$  to form the image embedding, where  $H$  and  $W$  are the height and width of the input degraded image. Both shallower and deeper stage selections perform worse (Appendix B.2). The condition encoder produces four embeddings: data-term and prior-term embeddings of  $d$  and  $r$ , respectively, and two optional MLP encodings of  $c$ —one for noise attributes if available (a multi-hot vector flagging which noise types are present, e.g., Gaussian alone or black-and-white impulse + Gaussian) and one for observation metadata if available (e.g., for Poisson–Gaussian low-light denoising, the read-noise  $\sigma$  and photon count are known and provided by camera calibration). If the observation metadata or

noise type is unavailable for a configuration, the corresponding MLP input is set to a fixed default vector. The four embeddings are concatenated with the image embedding. A 2-layer MLP then maps this concatenation to a feature  $\mathbf{h}$  used by the denoiser-calibrated slot readout described below.

**Denoiser-calibrated slot readout.** To maximize transferability, a label for one denoiser should help predict the same hyperparameter role in other denoisers, instead of supervising only that denoiser’s output. For example, a  $\lambda$  label in TV should help predict  $\lambda$  in TGV. The readout therefore assigns each recurring role to a shared slot of  $\mathbf{p}$ , so labels from any denoiser contribute to training that shared slot. However, the same role can have different numerical ranges across denoisers, so we design a denoiser-calibrated slot readout to scale and offset each slot’s prediction.

The slot embedding  $\mathbf{e}_j$  encodes the hyperparameter semantics of slot  $j$  and depends only on role and scale. Given configuration  $(d, r)$ , the role/scale lookup (Figure 2) assigns each slot  $j$  a role tag  $\rho_j \in \{\delta, \lambda, \gamma, \text{pad}\}$  and a scale tag  $\tau_j$  ( $\log_{10}$  for  $\lambda$ ; linear for  $\delta, \gamma$ ; none for padding). Two embedding matrices then map these tags to the corresponding slot embedding:

$$\mathbf{e}_j = \mathbf{E}_{\text{role}}[\rho_j] + \mathbf{E}_{\text{scale}}[\tau_j].$$

The projected feature  $\mathbf{U}\mathbf{h} + \mathbf{w}$  takes an inner product with the slot embedding  $\mathbf{e}_j$  to produce  $s_j$ . Because each slot can take different numerical ranges across denoisers, we apply a learned affine  $g_{d,r,j}s_j + b_{d,r,j}$  to scale and shift  $s_j$  into the range for each  $(d, r, j)$ .  $\mathbf{a}_j^\top \mathbf{h}$  provides a linear shortcut from  $\mathbf{h}$  directly into  $\hat{p}_j$ .

$$s_j = (\mathbf{U}\mathbf{h} + \mathbf{w})^\top \mathbf{e}_j, \quad \hat{p}_j = \underbrace{g_{d,r,j}s_j + b_{d,r,j}}_{\text{denoiser-calibrated shared score}} + \underbrace{\mathbf{a}_j^\top \mathbf{h}}_{\text{linear shortcut}}. \quad (3)$$

For log-scale slots,  $\hat{p}_j$  is mapped back to raw scale as  $10^{\hat{p}_j}$  before being output. Our ablation study in Appendix B.1 demonstrates the necessity of the proposed denoiser-calibrated slot readout.

### 2.3 Pooled Supervision

HyperDn is trained on oracle-labeled samples pooled across all source configurations. For each sample, the network predicts the full padded vector  $\hat{\mathbf{p}} \in \mathbb{R}^{L_{\text{max}}}$ , but the loss penalizes only the slots active for that sample’s  $(d, r)$ —for example,  $\lambda$  for TV;  $\delta$  and  $\lambda$  for Huber-TV;  $\lambda$  and  $\gamma$  for TGV. The exact regression loss is specified in Appendix A.

## 3 Experiments

### 3.1 Experimental Setups

**Goal.** We evaluate whether a single HyperDn can handle configurations not seen during source training. We conduct three experiments to evaluate transfer along three axes: few-shot transfer to a new prior term (DiffPIR), zero-shot transfer to unseen mixed noise (noise types seen individually in training), and zero-shot cross-resolution transfer. **Training Setup.** For each image–configuration pair, the oracle label is the PSNR-maximizing hyperparameter vector found by hierarchical grid search. The source pool is experiment-specific: the DiffPIR and cross-resolution transfer experiments share a 13-source non-DiffPIR checkpoint trained on  $96 \times 96$  and  $256 \times 256$  source images, while the mixed-noise transfer experiment trains one predictor per unseen mixed-noise target on the two single-noise source training sets for that target’s noise types. **Evaluation Setup.** We report reconstruction PSNR and the gap to oracle (oracle PSNR minus predictor PSNR), with mean  $\pm$  std over 5 seeds for learned methods. Table 1 summarizes the three transfer axes, and Appendix A gives denoiser specifications, source training sets, loss weighting, optimizer settings, and DiffPIR-specific details.

Table 1: Experiment overview.

Experiment	Transfer axis	Target labels	Main evidence
DiffPIR few-shot	new prior term	{1, 2, 4, 16, 32, 64, 128}	0.29 dB to oracle at 16 target labels
Mixed-noise transfer	unseen mixture of seen noise types	0	0.21/0.09 dB to oracle
Cross-resolution transfer	larger images	0	near-oracle across evaluated cells

### 3.2 Few-Shot Transfer to DiffPIR

We test how few DiffPIR target labels HyperDn needs to reach near-oracle quality, starting from a non-DiffPIR source-pretrained checkpoint. DiffPIR oracle labels require expensive diffusion sampling; therefore, transfer from the relatively cheap TV/TGV sources is practically valuable. The target configuration uses diffusion-based DiffPIR [Zhu et al., 2023] on  $256 \times 256$  crops from the Waterloo Exploration Database (WED) [Ma et al., 2017].

We compare three predictors across  $\{1, 2, 4, 16, 32, 64, 128\}$  DiffPIR target labels: **HyperDn** initialized from the source checkpoint, **HyperDn (ImageNet init only)** sharing the architecture but without source pretraining, and an **Afkham-style per-configuration CNN** [Afkham et al., 2021] trained from scratch on the target labels. The two HyperDn arms differ only in source pretraining; their performance gap measures how much source pretraining contributes. The CNN baseline reuses the prior work’s architecture, with the input channels extended from grayscale to RGB. All methods share the same sampler schedule and oracle construction.

HyperDn performs best across the full shot range (Figure 3; numbers in Appendix A). At 1 target label HyperDn is within 1.76 dB of the 31.13 dB oracle while the per-configuration CNN trails by 8.07 dB and the ImageNet-init arm by 6.15 dB. By 2 labels HyperDn is within 0.90 dB and outperforms the 64-label per-configuration CNN (30.23 vs. 29.92 dB), so HyperDn uses 1/32 as many target labels as that baseline point. By 4 labels HyperDn is within 0.51 dB; by 32 labels within 0.10 dB. Comparison with the same-architecture ImageNet-pretrained counterpart, HyperDn (ImageNet-init only), demonstrates the importance of source pretraining: the counterpart trails HyperDn by 4.39 dB with 1 label and 2.50 dB with 2 labels. Figure 4 shows 1-shot and 2-shot reconstruction samples for all methods.

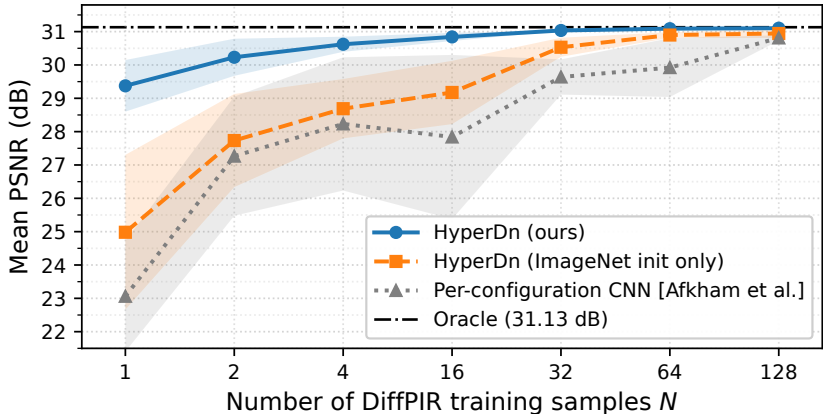


Figure 3: Few-shot transfer to DiffPIR on WED  $256 \times 256$  crops. Mean test-set PSNR (100 DiffPIR iterations) vs. the number of labeled DiffPIR training images; shaded bands are  $\pm$ std over 5 seeds. Oracle: 31.13 dB (dash-dot).

### 3.3 Zero-Shot Transfer to Mixed Noise

We test whether HyperDn handles unseen noise mixtures when trained only on single-noise labels. The number of possible noise mixtures grows combinatorially with the number of noise types, so labeling every mixture is expensive.

For each unseen mixed-noise target, all three methods use the same source data—the two single-noise source training sets for the target’s noise types—and evaluate directly on the mixture. The two targets are black-and-white (bw) impulse + Gaussian with Huber-TV and R/G/B (rgb) impulse + Gaussian with Huber-TGV. **HyperDn** pools both training sets into one. **CNN-mean** averages predicted hyperparameters of two Afkham-style per-configuration CNNs trained independently on each training set. **Mean-opt** computes one mean oracle hyperparameter vector per single-noise training set, then averages the two. These baselines test whether simply averaging single-noise predictions or optima is sufficient.

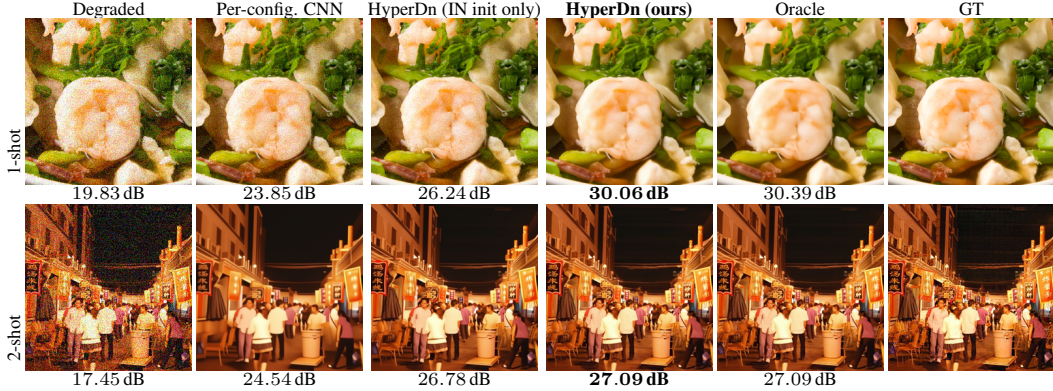


Figure 4: Reconstruction samples of few-shot transfer to DiffPIR on WED  $256 \times 256$  crops. Row 1: 1-shot (baselines under-denoise, leaving residual noise). Row 2: 2-shot (baselines over-smooth, washing out texture). HyperDn matches the oracle at 2-shot and stays within 0.33 dB at 1-shot.

HyperDn stays within 0.21 / 0.09 dB of the oracle on the two targets (Table 2, Figure 5), while CNN-mean and Mean-opt trail by 5–7 dB. This shows that HyperDn’s zero-shot mixed-noise transfer is not a trivial consequence of averaging single-noise predictors or optima.

Table 2: Zero-shot transfer to mixed-noise targets. Mean  $\pm$  std over 5 seeds for learned methods (Mean-opt and Oracle are deterministic).

Noise type (Denoiser)	CNN-mean	Mean-opt	HyperDn (Ours)	Oracle
bw impulse + Gaussian (Huber-TV)	17.44 $\pm$ 0.92	18.95	<b>24.31 <math>\pm</math> 0.07</b>	24.52
rgb impulse + Gaussian (Huber-TGV)	19.68 $\pm$ 0.86	17.91	<b>25.00 <math>\pm</math> 0.06</b>	25.09

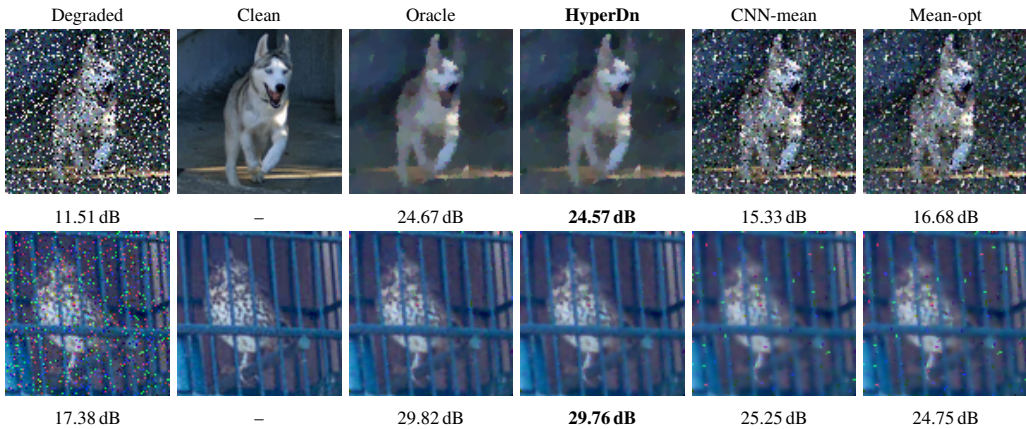


Figure 5: Reconstruction samples of zero-shot transfer to mixed noise. Top row: bw impulse + Gaussian with Huber-TV. Bottom row: rgb impulse + Gaussian with Huber-TGV. Both averaging baselines (CNN-mean, Mean-opt) leave residual noise; HyperDn matches the oracle on both targets.

### 3.4 Zero-Shot Cross-Resolution Transfer

We test whether HyperDn, source-pretrained jointly on the 13 small-image source training sets of §3.1 (12 STL10 [Coates et al., 2011]  $96 \times 96$  and 1 WED  $256 \times 256$  crops, spanning multiple denoiser/noise configurations), stays near-oracle on larger test images without any target labels. A  $512 \times 768$  Kodak24 oracle label costs roughly  $40 \times$  more denoiser time than a  $96 \times 96$  STL10 label, so transferring from cheap small-image labels to expensive large-image targets is practically valuable. Figure 6 illustrates this cross-resolution transfer.

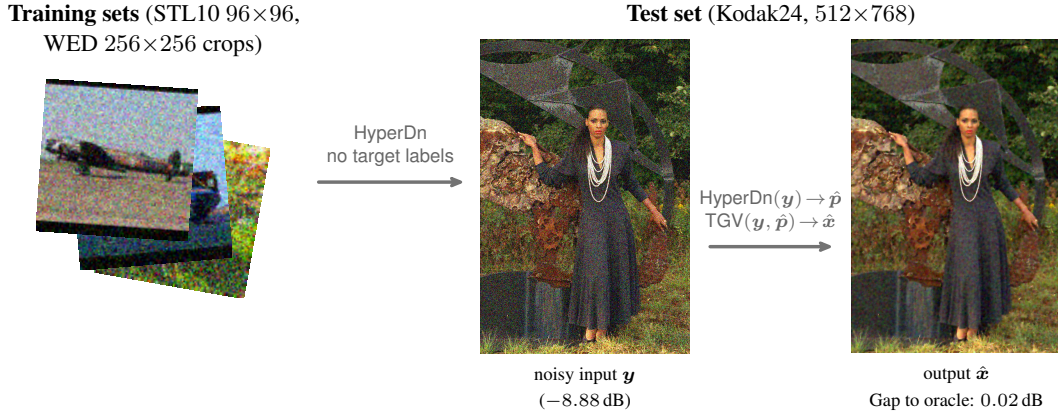


Figure 6: Zero-shot cross-resolution transfer. HyperDn is trained on small-image source training sets and applied directly to larger test images without any target labels. Given the noisy input  $y$ , HyperDn predicts  $\hat{p}$ , which the L2-TGV denoiser then uses to produce the reconstruction image  $\hat{x}$ .

We evaluate three configurations on Kodak24 [Eastman Kodak Company, 1999]; for L2-TV with Gaussian we additionally evaluate on CBS68 [Martin et al., 2001] and Urban100 [Huang et al., 2015].

HyperDn stays near-oracle in every evaluated cell (Table 3), showing zero-shot transfer from small source images to larger target images.

Table 3: Zero-shot cross-resolution transfer. HyperDn is the 13-source jointly pretrained checkpoint of §3.1 (12 STL10 96×96 + 1 WED 256×256 crops), applied directly to each target without finetuning. “Gap to oracle” is the mean over test images of (oracle PSNR – HyperDn PSNR);  $\pm$  is the standard deviation across random seeds.

Configuration	Noise	Dataset	Resolution	Gap to oracle ↓
Huber-TV	bw impulse	Kodak24	512×768	0.06±0.06
L2-TGV	Gaussian	Kodak24	512×768	0.02±0.01
L2-TV	Gaussian	CBS68	321×481	0.01±0.0029
		Kodak24	512×768	0.27±0.0030
		Urban100	~1024×768	0.02±0.0045

## 4 Related Work

**Hyperparameter selection.** Classical parameter-selection rules include the L-curve [Hansen, 1992] and generalized cross-validation [Golub et al., 1979]. Prior work on imaging hyperparameter selection includes predicting regularization parameters [Afkham et al., 2021], learning spatially varying TGV parameters [Vu et al., 2025], tuning-free plug-and-play rules [Wei et al., 2020], and bilevel parameter learning for variational imaging [los Reyes et al., 2017]. These methods choose or learn parameters within a given denoising model or algorithm setting. The relevant classical comparator for our experiments is Monte-Carlo SURE [Ramani et al., 2008], because it provides per-image parameter tuning for additive Gaussian denoising with known or estimable variance. The Monte-Carlo SURE comparator used here is limited to additive-Gaussian denoising with known Gaussian noise level. Appendix C compares SURE and HyperDn on the L2-TV + Gaussian configuration. We are not aware of prior work that transfers oracle supervision to train a single hyperparameter predictor reusable across many denoising configurations. HyperDn instead transfers oracle supervision across configurations with a single predictor. This is the setting that motivates HyperDn.

**Learned hyperparameter optimization across tasks.** Learned hyperparameter optimization transfers information from past hyperparameter searches: FSBO [Wistuba and Grabocka, 2021], OptFormer [Chen et al., 2022], and ranking-weighted Gaussian process ensembles [Feurer et al., 2018] suggest new trials for a target task. These methods evaluate target-task trial responses during search;

HyperDn instead uses oracle supervision from the training sets and predicts  $\hat{p}$  from the degraded input image at deployment, requiring no target clean image or target-task oracle evaluation.

**Hypernetworks and conditional parameter generation.** Hypernetworks generate the weights of another neural network [Ha et al., 2017], while dynamic-filter networks generate input-conditioned filters [Jia et al., 2016]. HyperRecon [Wang et al., 2022] uses a hypernetwork to compute multiple image reconstructions across hyperparameter settings. HyperDn does not generate any network weights. It predicts the active hyperparameters for a fixed model-based denoiser under a queried configuration. We then ask whether oracle hyperparameter supervision transfers across configurations.

**Meta-learning.** Gradient-based meta-learning methods such as MAML [Finn et al., 2017], Reptile [Nichol et al., 2018], and their variants learn an initialization that can be adapted to a new task with a few gradient steps on target labels. HyperDn instead trains one configuration-conditioned predictor on pooled oracle labels across source configurations, then runs a single forward pass at deployment. In the zero-shot experiments of §3.3 and §3.4, it needs neither an inner loop nor any target labels. The few-shot DiffPIR study in §3.2 uses standard supervised finetuning of this predictor, not the inner loop of a meta-learned fast-adaptation initialization.

## 5 Conclusion and Discussion

We demonstrate that oracle hyperparameter supervision transfers across denoising configurations. HyperDn, a single configuration-conditioned predictor trained on oracle labels pooled across source configurations, transfers along three axes, each in a cost-asymmetric direction that saves expensive labeling. First, from relatively cheap TV/TGV oracle labels to more expensive DiffPIR oracle labels: with only 2 DiffPIR target labels, HyperDn comes within 0.90 dB of the 31.13 dB oracle and outperforms the 64-label per-configuration predictor trained from scratch, using 1/32 as many target labels as that baseline point. Second, from single-noise sources to their mixed-noise targets: HyperDn predicts mixture hyperparameters with no target labels, reducing the need to label every possible mixture. Third, from relatively cheap small-image sources to more expensive high-resolution test images: HyperDn stays near-oracle with no target labels, replacing oracle labels that cost roughly  $40\times$  more denoiser time at  $512\times 768$  than at  $96\times 96$ . Together, these results show that oracle supervision can transfer effectively across denoising configurations, reducing the expensive oracle search needed for each new configuration.

**Limitations.** HyperDn is designed for cross-configuration transfer within the model-based denoising settings studied here. The new denoiser transfer is few-shot rather than zero-shot: it substantially reduces target-side oracle labeling, but still uses a small number of target labels for finetuning. The zero-target-label mixed-noise results are limited to mixtures whose component noise types are seen separately under the same denoising model. The zero-target-label cross-resolution results are most effective when source and target images share similar local structure. We provide empirical evidence rather than a formal guarantee that cross-configuration transfer will hold outside the tested settings. At deployment, HyperDn runs as a single forward pass through its 2.18M-parameter backbone, so per-image inference cost is dominated by the downstream denoising solver. Training compute is dominated by source-side oracle label generation, which keeps its  $t_{\text{call}} \times K_{\text{sweep}} \times N_{\text{img}} \times N_{\text{cfg}}$  scaling; HyperDn does not reduce this source-side cost.

**Broader impacts.** On the positive side, HyperDn lowers the oracle-label cost that gates practical deployment of model-based denoising and lets researchers reuse shared supervision when iterating on new regularizers or data terms. On the negative side, broader deployment of model-based denoising may aid privacy-sensitive surveillance or forensic enhancement. HyperDn adds no generation, identification, or data-collection capability, so this risk is inherited from denoising rather than introduced by the hyperparameter-transfer method.

**Future work.** A natural next step is to train a single predictor on a much larger pool of oracle-labeled source configurations, broad enough that most new configurations need only a few target labels. The present paper is a first step toward that broader predictor, on a small slice of the configuration space.

## References

- Babak Maboudi Afkham, Julianne Chung, and Matthias Chung. Learning regularization parameters of inverse problems via deep neural networks. *Inverse Problems*, 37(10):105017, 2021. doi: 10.1088/1361-6420/ac245d.
- Stephen Boyd, Neal Parikh, Eric Chu, Borja Peleato, and Jonathan Eckstein. Distributed optimization and statistical learning via the alternating direction method of multipliers. *Foundations and Trends in Machine Learning*, 3(1):1–122, 2011. doi: 10.1561/22000000016. URL <https://doi.org/10.1561/22000000016>.
- Kristian Bredies, Karl Kunisch, and Thomas Pock. Total generalized variation. *SIAM Journal on Imaging Sciences*, 3(3):492–526, 2010. doi: 10.1137/090769521.
- Yutian Chen, Xingyou Song, Chansoo Lee, Zi Wang, Qiuyi Zhang, David Dohan, Kazuya Kawakami, Greg Kochanski, Arnaud Doucet, Marc’Aurelio Ranzato, Sagi Perel, and Nando de Freitas. Towards learning universal hyperparameter optimizers with transformers. In *Advances in Neural Information Processing Systems (NeurIPS)*, 2022. URL [https://proceedings.neurips.cc/paper\\_files/paper/2022/hash/cf6501108fced72ee5c47e2151c4e153-Abstract-Conference.html](https://proceedings.neurips.cc/paper_files/paper/2022/hash/cf6501108fced72ee5c47e2151c4e153-Abstract-Conference.html).
- Adam Coates, Andrew Y. Ng, and Honglak Lee. An analysis of single-layer networks in unsupervised feature learning. In *Proceedings of the Fourteenth International Conference on Artificial Intelligence and Statistics*, volume 15 of *Proceedings of Machine Learning Research*, pages 215–223. PMLR, 2011. URL <https://proceedings.mlr.press/v15/coates11a.html>.
- Jia Deng, Wei Dong, Richard Socher, Li-Jia Li, Kai Li, and Li Fei-Fei. ImageNet: A large-scale hierarchical image database. In *IEEE Conference on Computer Vision and Pattern Recognition (CVPR)*, pages 248–255, 2009. doi: 10.1109/CVPR.2009.5206848.
- Eastman Kodak Company. Kodak Lossless True Color Image Suite (PhotoCD PCD0992). <http://r0k.us/graphics/kodak/>, 1999. URL <http://r0k.us/graphics/kodak/>.
- Matthias Feurer, Benjamin Letham, Frank Hutter, and Eytan Bakshy. Practical transfer learning for Bayesian optimization, 2018. URL <https://arxiv.org/abs/1802.02219>.
- Chelsea Finn, Pieter Abbeel, and Sergey Levine. Model-agnostic meta-learning for fast adaptation of deep networks. In *Proceedings of the International Conference on Machine Learning (ICML)*, volume 70 of *Proceedings of Machine Learning Research*, pages 1126–1135. PMLR, 2017. URL <https://proceedings.mlr.press/v70/finn17a.html>.
- Tom Goldstein and Stanley Osher. The split bregman method for  $l_1$ -regularized problems. *SIAM Journal on Imaging Sciences*, 2(2):323–343, 2009. doi: 10.1137/080725891.
- Gene H. Golub, Michael Heath, and Grace Wahba. Generalized cross-validation as a method for choosing a good ridge parameter. *Technometrics*, 21(2):215–223, 1979. doi: 10.1080/00401706.1979.10489751. URL <https://doi.org/10.1080/00401706.1979.10489751>.
- David Ha, Andrew Dai, and Quoc V. Le. Hypernetworks. In *International Conference on Learning Representations (ICLR)*, 2017. URL <https://openreview.net/forum?id=rkpACe1lx>.
- Per Christian Hansen. Analysis of discrete ill-posed problems by means of the L-curve. *SIAM Review*, 34(4):561–580, 1992. doi: 10.1137/1034115. URL <https://doi.org/10.1137/1034115>.
- Jeremy Howard and Sebastian Ruder. Universal language model fine-tuning for text classification. In *Proceedings of the 56th Annual Meeting of the Association for Computational Linguistics (Volume 1: Long Papers)*, pages 328–339, 2018. doi: 10.18653/v1/P18-1031. URL <https://aclanthology.org/P18-1031/>.
- Jia-Bin Huang, Abhishek Singh, and Narendra Ahuja. Single image super-resolution from transformed self-exemplars. In *IEEE Conference on Computer Vision and Pattern Recognition (CVPR)*, pages 5197–5206, 2015. doi: 10.1109/cvpr.2015.7299156. URL <https://doi.org/10.1109/cvpr.2015.7299156>.

- Xu Jia, Bert De Brabandere, Tinne Tuytelaars, and Luc Van Gool. Dynamic filter networks. In *Advances in Neural Information Processing Systems (NeurIPS)*, pages 667–675, 2016. URL <https://papers.nips.cc/paper/2016/hash/8bf1211fd4b7b94528899de0a43b9fb3-Abstract.html>.
- Alex Kendall, Yarin Gal, and Roberto Cipolla. Multi-task learning using uncertainty to weigh losses for scene geometry and semantics. In *Proceedings of the IEEE/CVF Conference on Computer Vision and Pattern Recognition (CVPR)*, pages 7482–7491, 2018. doi: 10.1109/CVPR.2018.00781.
- J. C. De los Reyes, Carola-Bibiane Schönlieb, and Tuomo Valkonen. Bilevel parameter learning for higher-order total variation regularisation models. *Journal of Mathematical Imaging and Vision*, 57(1):1–25, 2017. doi: 10.1007/s10851-016-0662-8.
- Ilya Loshchilov and Frank Hutter. Decoupled weight decay regularization. In *International Conference on Learning Representations (ICLR)*, 2019. URL <https://openreview.net/forum?id=Bkg6RiCqY7>.
- Kede Ma, Zhengfang Duanmu, Qingbo Wu, Zhou Wang, Hongwei Yong, Hongliang Li, and Lei Zhang. Waterloo Exploration Database: New challenges for image quality assessment models. *IEEE Transactions on Image Processing*, 26(2):1004–1016, 2017. doi: 10.1109/TIP.2016.2631888.
- David R. Martin, Charless C. Fowlkes, Doron Tal, and Jitendra Malik. A database of human segmented natural images and its application to evaluating segmentation algorithms and measuring ecological statistics. In *Proceedings of the IEEE International Conference on Computer Vision (ICCV)*, volume 2, pages 416–423, 2001. doi: 10.1109/ICCV.2001.937655. URL <https://doi.org/10.1109/ICCV.2001.937655>.
- Alex Nichol, Joshua Achiam, and John Schulman. On first-order meta-learning algorithms, 2018. URL <https://arxiv.org/abs/1803.02999>.
- S. Ramani, T. Blu, and M. Unser. Monte-Carlo SURE: A black-box optimization of regularization parameters for general denoising algorithms. *IEEE Transactions on Image Processing*, 17(9):1540–1554, 2008. doi: 10.1109/TIP.2008.2001404.
- Leonid I. Rudin, Stanley Osher, and Emad Fatemi. Nonlinear total variation based noise removal algorithms. *Physica D: Nonlinear Phenomena*, 60(1–4):259–268, 1992. doi: 10.1016/0167-2789(92)90242-f. URL [https://doi.org/10.1016/0167-2789\(92\)90242-f](https://doi.org/10.1016/0167-2789(92)90242-f).
- Thanh Trung Vu, Andreas Kofler, and Kostas Papafitsoros. Deep unrolling for learning optimal spatially varying regularisation parameters for total generalised variation. In *Lecture Notes in Computer Science*, pages 282–294. Springer Nature Switzerland, 2025. doi: 10.1007/978-3-031-92366-1\_22. URL <https://arxiv.org/abs/2502.16532>.
- Alan Q. Wang, Adrian V. Dalca, and Mert R. Sabuncu. Computing multiple image reconstructions with a single hypernetwork. *Machine Learning for Biomedical Imaging*, 1(June 2022 issue):1–25, 2022. doi: 10.59275/j.melba.2022-e5ec. URL <https://melba-journal.org/2022:017>.
- Kaixuan Wei, Angelica I. Aviles-Rivero, Jingwei Liang, Ying Fu, Carola-Bibiane Schönlieb, and Hua Huang. Tuning-free plug-and-play proximal algorithm for inverse imaging problems. In *Proceedings of the International Conference on Machine Learning (ICML)*, volume 119 of *Proceedings of Machine Learning Research*, pages 10158–10169. PMLR, 2020. URL <https://proceedings.mlr.press/v119/wei20b.html>.
- Martin Wistuba and Josif Grabocka. Few-shot Bayesian optimization with deep kernel surrogates. In *International Conference on Learning Representations (ICLR)*, 2021. URL <https://openreview.net/forum?id=bJxgv5C3sYc>.
- Sanghyun Woo, Shoubhik Debnath, Ronghang Hu, Xinlei Chen, Zhuang Liu, In So Kweon, and Saining Xie. Convnext v2: Co-designing and scaling convnets with masked autoencoders. In *Proceedings of the IEEE/CVF Conference on Computer Vision and Pattern Recognition (CVPR)*, pages 16133–16142, 2023. doi: 10.1109/cvpr52729.2023.01548. URL <https://doi.org/10.1109/cvpr52729.2023.01548>.

Yuanzhi Zhu, Kai Zhang, Jingyun Liang, Jiezhong Cao, Bihan Wen, Radu Timofte, and Luc Van Gool. Denoising diffusion models for plug-and-play image restoration. In *IEEE/CVF Conference on Computer Vision and Pattern Recognition Workshops (CVPRW)*, pages 1219–1229, 2023. doi: 10.1109/cvprw59228.2023.00129. URL <https://doi.org/10.1109/cvprw59228.2023.00129>.

The appendix is organized to support the claims made in the main paper. Section A records the experimental details, loss weighting, and additional DiffPIR numbers behind the transfer experiments. Section B reports the two architecture-validation ablations referenced in the method section: the denoiser-calibrated slot readout and the backbone stage selection. Section C provides the restricted classical comparison against SURE on the L2-TV Gaussian axis.

## A Experimental Details and Additional Results

Here we record the training, evaluation, and reporting choices behind the transfer experiments in Section 3. The details below cover the oracle construction, loss weighting, and precise numbers behind the DiffPIR few-shot figure.

**Oracle construction and loss weighting.** All experiments use oracle labels produced by hierarchical grid searches, with the target hyperparameter vector defined as the PSNR-maximizing setting for each image-configuration pair. All three transfer experiments train by regression over the active slots, as described in Section 2.3. For a configuration  $\chi$ , let  $\mathcal{A}_\chi$  be the set of slots that are real hyperparameters rather than padding. For training configurations  $\mathcal{C}_{\text{tr}}$  and labeled examples  $\mathcal{D}_\chi$  from configuration  $\chi$ , the unweighted objective is

$$\mathcal{L}_{\text{slot}}(\Theta) = \frac{1}{Z} \sum_{\chi \in \mathcal{C}_{\text{tr}}} \sum_{u \in \mathcal{D}_\chi} \sum_{j \in \mathcal{A}_\chi} (\hat{p}_{\chi,u,j} - p_{\chi,u,j}^*)^2, \quad Z = \sum_{\chi \in \mathcal{C}_{\text{tr}}} \sum_{u \in \mathcal{D}_\chi} |\mathcal{A}_\chi|. \quad (4)$$

The zero-shot mixed-noise runs use this plain active-slot MSE. The main joint pretraining run and the DiffPIR few-shot finetuning stage use the homoscedastic role weighting of Kendall et al. [2018]. Let  $s_\rho = \log \sigma_\rho^2$  be the learned log-variance for parameter role  $\rho$ , and let  $\rho_{\chi,j}$  be the role of active slot  $j$  under configuration  $\chi$ . The weighted objective is

$$\mathcal{L}_{\text{role}}(\Theta, \mathbf{s}) = \frac{1}{Z} \sum_{\chi \in \mathcal{C}_{\text{tr}}} \sum_{u \in \mathcal{D}_\chi} \sum_{j \in \mathcal{A}_\chi} \left[ \frac{1}{2} \exp(-s_{\rho_{\chi,j}}) (\hat{p}_{\chi,u,j} - p_{\chi,u,j}^*)^2 + \frac{1}{2} s_{\rho_{\chi,j}} \right]. \quad (5)$$

This loss matches the Gaussian negative log-likelihood form up to constants independent of  $\Theta$  and  $\mathbf{s}$ . For source-pretrained HyperDn, DiffPIR finetuning inherits the pretrained log-variances, so source pretraining and target finetuning use the same weighting parameters.

**Solver specifications.** The fixed denoisers used for oracle-label generation and test-time reconstruction are:

- **L2-TV denoising:** `skimage.restoration.denoise_tv_bregman` wrapped as a normalized TV solver, based on the split Bregman method [Goldstein and Osher, 2009]. The wrapper uses isotropic TV, per-channel weight  $1/(2\lambda)$ , and scikit-image’s default termination criterion (`max_num_iter=100`, `eps=10-3`; the inner Bregman loop terminates at whichever bound is reached first). This solver is used in Appendix C and in the L2-TV cross-resolution cell.
- **Huber-TV denoising** (used for the Huber-TV mixed-noise target and its single-noise training sets): the same skeleton based on the alternating direction method of multipliers [Boyd et al., 2011], with a Huber data prox. It uses fixed 100 iterations,  $\rho_{\text{TV}}=2.0$ ,  $\rho_{\text{data}}=5.0$ . The active parameters are the Huber threshold  $\delta$  and the TV weight  $\lambda$ .
- **L2/NLL-TGV denoising** (used for the L2-TGV cross-resolution cell and the TGV source training sets without a Huber data term): second-order TGV with active parameters  $(\lambda, \gamma)$ , where  $\lambda$  controls regularization strength and  $\gamma$  is the second-order to first-order weight ratio. In the denoising wrapper this corresponds to  $\alpha_1 = \lambda$  and  $\alpha_0 = \gamma\lambda$ , with 120 fixed iterations.
- **Huber-TGV denoising** (used for the Huber-TGV mixed-noise target and Huber-TGV source training sets): the same TGV regularizer, but with a Huber data term. The active parameters are  $(\delta, \lambda, \gamma)$ , with  $\delta$  passed as the Huber threshold.

The four denoisers above run on CPU and are deterministic (no random sampling inside the solver), so repeated oracle sweeps give identical labels. Termination: L2-TV uses scikit-image’s default split-Bregman criterion above; Huber-TV uses fixed 100 iterations; L2/NLL-TGV and Huber-TGV use fixed 120 iterations. The DiffPIR few-shot setting uses the public DiffPIR sampler at 100 iterations as described in §3.2 and the evaluation details below.

**Noise sampling.** For every experiment, each clean image receives one randomly sampled noise realization with a deterministic per-image seed, used identically across the oracle sweep, training, and evaluation:

- **Gaussian noise (DiffPIR few-shot target on WED 256×256 crops, Gaussian source training sets, and classical-comparison test sets):** per-image standard deviation  $\sigma \sim \text{Uniform}(5/255, 50/255)$ , applied additively per pixel.
- **Black-and-white impulse (Huber-TV “bw impulse” source and cross-resolution target):** channel-shared salt-and-pepper with amount  $\sim \text{Uniform}(0.05, 0.30)$  and salt/pepper ratio 0.5.
- **RGB impulse (Huber-TGV “rgb impulse” source and mixed-noise target):** channel-independent salt-and-pepper with the same amount range  $\sim \text{Uniform}(0.05, 0.30)$  and salt/pepper ratio 0.5.
- **Poisson and Poisson–Gaussian (NLL source training sets):** per-image photon scale is sampled as  $p_{\max} \sim \text{Uniform}(2, 128)$  with  $\alpha = 1/p_{\max}$  in the Poisson observation model. Pure Poisson uses read noise  $\sigma_{\text{read}} = 0$ , while Poisson–Gaussian samples  $\sigma_{\text{read}} \sim \text{Uniform}(0.5/255, 16/255)$ ; the background offset is fixed to 0.
- **Mixed-noise configurations (Huber-TV bw impulse + Gaussian, Huber-TGV rgb impulse + Gaussian):** each noise type is sampled independently from its single-noise range above and applied in sequence (impulse, then Gaussian).

The Kodak24 512×768 target for the L2-TGV cross-resolution cell uses the same Gaussian noise range as its matching STL10 source training set, so the noise range is matched while the target images are larger and come from Kodak24. The cross-resolution Huber-TV bw impulse target on Kodak24 likewise uses the same impulse-amount range as its matching STL10 source training set.

**Main joint pretraining run.** The source-pretrained checkpoint used for DiffPIR few-shot transfer and zero-shot cross-resolution transfer is trained on the 13 non-DiffPIR source training sets in Table 4: 12 STL10 96×96 and 1 WED 256×256 crops, spanning Gaussian, Poisson, Poisson–Gaussian, and bw/rgb impulse noise (alone or mixed with Gaussian). The architecture is ConvNeXtV2-base [Woo et al., 2023] pretrained on ImageNet, restricted to the stem and stages 0–1, combined with a denoiser-calibrated slot readout ( $L_{\max}=3$  output slots, sized to fit Huber-TGV’s  $(\delta, \lambda, \gamma)$ ); 32-dim role/scale embeddings, 16-dim metadata embeddings, two-layer GELU trunk MLP with LayerNorm and 512-dim hidden output  $\mathbf{h}$ , dropout 0.1, and one learned log-variance parameter  $\log \sigma^2$  per output role for the uncertainty-based weighting). The bilinear part  $(\mathbf{U}\mathbf{h})^\top \mathbf{e}_j$  of the score in Eq. (3) is implemented as the inner product of two projections  $\mathbf{q} = \mathbf{Q}\mathbf{h} \in \mathbb{R}^{128}$  ( $\mathbf{Q} \in \mathbb{R}^{128 \times 512}$ ) and  $\mathbf{k}_j = \mathbf{K}\mathbf{e}_j \in \mathbb{R}^{128}$  ( $\mathbf{K} \in \mathbb{R}^{128 \times 32}$ ), so  $\mathbf{U} = \mathbf{K}^\top \mathbf{Q} \in \mathbb{R}^{32 \times 512}$  is factored through a 128-dim shared bilinear space; the role/scale-dependent offset  $\mathbf{w}^\top \mathbf{e}_j$  is realized through the bias of these projections. We optimize with AdamW [Loshchilov and Hutter, 2019]. The run uses 80 epochs at batch size 128, layer-wise learning-rate decay (LLRD) [Howard and Ruder, 2018] 0.8, head LR  $2 \times 10^{-4}$ , weight decay  $10^{-5}$ , cosine schedule to  $10^{-6}$  after 10% linear warmup, gradient clipping at 1.0, and mixed precision. Augmentations are random horizontal/vertical flips and 90°/270° rotations; we apply no condition-embedding dropout and report results over 5 random-initialization seeds. We hold out 5% of each source as validation and select the checkpoint with the lowest validation weighted loss. Each training batch draws from a single source instead of mixing sources, so we can balance the per-source mean loss across sources of very different sizes.

**DiffPIR few-shot finetuning.** Both HyperDn arms share the same DiffPIR finetuning schedule on the target side: 150 epochs, head learning rate  $\text{LR}_{\text{head}} = 10^{-4}$ , LLRD decay 0.1 (backbone effectively frozen; head and embeddings adapt), 30% linear warmup, batch size at most 8 (or the target-label count when smaller), AdamW with weight decay  $10^{-5}$  and gradient clipping at 1.0, no mixed precision, and the same uncertainty-based weighting form used during pretraining. Because the target-label count is small, we use no validation split and select the last-epoch checkpoint. HyperDn (ours) initializes from the *full* source-pretrained checkpoint (backbone, head, embeddings, and weighting parameters). The DiffPIR scale and bias parameters  $g_{d,\text{DIFFPIR},j}$  and  $b_{d,\text{DIFFPIR},j}$  sit at their identity init ( $g=1, b=0$ ) when target finetuning begins. DiffPIR rows exist in the source-pretrained embedding tables, but no source training set activates them, so source-pretraining gradients never update them; the tables are loaded verbatim into the target-finetuning model, and the DiffPIR

Table 4: Non-DiffPIR source training sets used for the joint-pretrained checkpoint. “bw” and “rgb” denote black-and-white and channel-wise impulse noise; NLL denotes the likelihood-based data term used for Poisson or Poisson–Gaussian observations.

#	Dataset/res.	Noise	Data term	Regularizer
1	STL10 96×96	bw impulse + Gaussian	Huber	TV
2	STL10 96×96	bw impulse	Huber	TGV
3	STL10 96×96	bw impulse	Huber	TV
4	STL10 96×96	Gaussian	Huber	TGV
5	STL10 96×96	Gaussian	L2	TGV
6	STL10 96×96	Gaussian	L2	TV
7	WED 256×256 crops	Gaussian	L2	TV
8	STL10 96×96	Gaussian	Huber	TV
9	STL10 96×96	Poisson–Gaussian	NLL	TGV
10	STL10 96×96	Poisson–Gaussian	NLL	TV
11	STL10 96×96	Poisson	NLL	TV
12	STL10 96×96	rgb impulse + Gaussian	Huber	TGV
13	STL10 96×96	rgb impulse	Huber	TGV

rows adapt only during finetuning. HyperDn (ImageNet init only) loads the ImageNet-pretrained ConvNeXtV2 backbone and uses a randomly initialized head (seeded per run).

**Per-configuration CNN baseline.** The per-configuration CNN trains from random initialization on each shot/seed. Following the convolutional design of Afkham et al. [2021], adapted from the original single-channel deblurring setting to RGB DiffPIR denoising, this baseline uses a target-only neural network to predict regularization parameters for one inverse-problem configuration. It consists of three convolutional blocks (Conv 5×5, padding 2 → BatchNorm → ReLU → MaxPool 2×2, with channel widths 3→16→32→64), an adaptive average pool to 4×4, and an MLP head with hidden widths 1024→256→128→64 and ReLU between hidden layers, followed by a linear output for the active DiffPIR target; this is approximately 369 K parameters in total.

**DiffPIR reconstruction and evaluation.** DiffPIR reconstruction uses 100 iterations for label generation, oracle sweeps, and test-time evaluation, the same setting used to produce the  $\log_{10} \lambda$  oracle labels. The fidelity weight  $\zeta$  is fixed to 1.0 for every method across training labels, oracle sweep, and evaluation, so only the log-scale prior weight  $\log_{10} \lambda$  is predicted. We adopted  $\zeta=1.0$  from a preliminary joint sweep over prior weight  $\lambda$  and fidelity weight  $\zeta$  on all 4344 WED 256×256 training images, using a coarse  $\zeta$  grid plus local refinement. The training sweep alone selects  $\zeta=1.0$ : every one of the 4344 training images picks  $\zeta=1.0$  as its per-image PSNR optimum, so the choice uses no validation or test data. Agreement on the full 400-image validation split then confirms this choice rather than driving it. All methods (HyperDn, the ImageNet-init variant, and the per-configuration CNN baseline) and all uses (label generation, oracle sweep, test evaluation) fix  $\zeta=1.0$ , so this choice cannot bias the cross-method comparison in Table 5. Test-set PSNR in Table 5 is computed on a fixed, deterministic 50-image subset of the 400-image DiffPIR validation split, so all methods and seeds are compared on identical degraded inputs. PSNR is computed on float  $[0, 1]$  arrays without border cropping. Oracle PSNR on this subset is 31.13 dB.

**Precise numbers behind Figure 3.** Table 5 gives the exact values behind the few-shot transfer curve in Section 3.2: per-shot PSNR mean  $\pm$  std and gap to the 31.13 dB oracle for all three methods.

Table 5: Precise numbers for Figure 3: per-shot PSNR (mean  $\pm$  std, 5 seeds) and gap to the 31.13 dB oracle. The Per-configuration baseline has high seed-to-seed variance at intermediate label counts; best per shot in **bold**.

Labels	Reconstruction PSNR (dB) $\uparrow$			Gap to oracle (dB) $\downarrow$		
	Per-configuration	HyperDn		Per-configuration	HyperDn	
		(IN init only)	<b>HyperDn (ours)</b>		(IN init only)	<b>HyperDn (ours)</b>
1	23.06 $\pm$ 1.66	24.98 $\pm$ 2.32	<b>29.37 <math>\pm</math> 0.77</b>	8.07	6.15	<b>1.76</b>
2	27.26 $\pm$ 1.79	27.73 $\pm$ 1.40	<b>30.23 <math>\pm</math> 0.56</b>	3.87	3.40	<b>0.90</b>
4	28.23 $\pm$ 2.00	28.69 $\pm$ 0.89	<b>30.62 <math>\pm</math> 0.23</b>	2.90	2.44	<b>0.51</b>
16	27.84 $\pm$ 2.46	29.17 $\pm$ 0.95	<b>30.84 <math>\pm</math> 0.12</b>	3.29	1.96	<b>0.29</b>
32	29.64 $\pm$ 0.53	30.53 $\pm$ 0.29	<b>31.03 <math>\pm</math> 0.01</b>	1.50	0.60	<b>0.10</b>
64	29.92 $\pm$ 0.88	30.90 $\pm$ 0.09	<b>31.09 <math>\pm</math> 0.01</b>	1.21	0.23	<b>0.04</b>
128	30.81 $\pm$ 0.08	30.94 $\pm$ 0.14	<b>31.10 <math>\pm</math> 0.01</b>	0.32	0.19	<b>0.03</b>

**Zero-shot mixed-noise runs.** Each zero-shot run trains one model per mixed-noise target, using two single-noise source training sets drawn from the STL10 *train* split (5 000 images at  $96 \times 96$ ). Mixed-noise target evaluation in Table 2 is on the STL10 *test* split (8 000 images at  $96 \times 96$ ); no target oracle labels are seen during training. We use AdamW, head LR  $2 \times 10^{-4}$ , LLRD 0.8, weight decay  $10^{-5}$ , a cosine schedule with 10% warmup, mixed precision, 80 epochs, random horizontal/vertical flips and  $90/270^\circ$  rotations, no condition-embedding dropout, and batch size 256. The loss is plain MSE over the active parameter dimensions, with no additional uncertainty-based reweighting in this experiment. The multi-hot noise-attribute code has six slots: (unknown, has-Gaussian, has-Poisson, has-impulse, impulse-is-bw, impulse-is-rgb). Thus bw impulse + Gaussian encodes to  $[0, 1, 0, 1, 1, 0]$ , and rgb impulse + Gaussian encodes to  $[0, 1, 0, 1, 0, 1]$ .

**Evaluation reporting and hardware.** Predictor training and evaluation run on 1–5 NVIDIA RTX 4090 GPUs (24 GB VRAM each) in parallel across seeds and configurations, with one card per run. One main-run seed trains the 13-source pretraining run in  $\sim 2.5$  hours. DiffPIR few-shot finetuning takes  $\leq 1$  minute for  $\leq 32$  target labels and up to  $\sim 30$  minutes for 128 target labels per (seed, method) combination. Oracle-label generation is the costly stage. Non-DiffPIR TV/TGV labels are CPU-bound and embarrassingly parallel; in the paper run, the full 13-source sweep was sharded on a shared CPU cluster with approximately 600 CPU cores available and about 2 GB RAM per core, over roughly 10 days of elapsed wall-clock time. DiffPIR target-label generation for the 4344 WED  $256 \times 256$  training images is GPU-bound; in the paper run, these labels were generated on a heterogeneous, dynamically scheduled pool of 8–16 NVIDIA L40S and A100 GPUs over roughly 2 days of elapsed wall-clock time. The classical-method comparison (Table 9) reports per-image wall-clock time on the same machine. HyperDn inference is a single GPU forward pass and costs much less than the downstream CPU TV solver. SURE and the oracle sweep both require many CPU TV solver calls per image.

**Batched inference throughput.** To time inference, we benchmark the pure GPU forward pass under FP32, processing the entire uniform-shape test set as one batch. We use three uniform-shape sets at three resolutions: WED  $256 \times 256$  (natively uniform), CBSD68 at  $321 \times 481$ , and Kodak24 at  $512 \times 768$ . For CBSD68 and Kodak24, we rotate portrait images  $90^\circ$  to landscape so the whole set stacks into one batch; this batching-only rotation is used only for timing. Table 6 reports single-batch timing, throughput, and peak GPU memory for each set. At  $256 \times 256$ , the per-image forward drops to 0.78 ms (1280 img/s). At  $512 \times 768$ , the single forward is compute-bound, so throughput scales inversely with pixel count (212 img/s). Per-batch wall-clock time for the entire test set is 0.11–0.31 s in all three cases. The per-image numbers here are smaller than the corresponding entries in Table 9. That table measures full end-to-end per-call latency (including CPU→GPU transfer and Python-side overhead), while the appendix numbers isolate GPU compute. Under either approach, HyperDn inference is dominated by the downstream CPU TV solver and is effectively free at deployment scale.

Table 6: HyperDn single-batch throughput (FP32). Each row processes a uniform-shape test set as one batch of size  $bs$ ; CBSD68 and Kodak24 are rotated to a uniform landscape shape, and WED is natively uniform. “Mem/img” divides peak forward memory by  $bs$ , so fixed model weights are shared across the batch.

Dataset	Shape	$bs$	Batch time (ms)	Per-image (ms)	Throughput (img/s)	Mem/img
WED (center-cropped)	$256 \times 256$	400	$312.5 \pm 6.8$	0.78	1280	31 MB
CBSD68	$321 \times 481$	68	$124.4 \pm 0.8$	1.83	547	73 MB
Kodak24	$512 \times 768$	24	$113.1 \pm 1.0$	4.71	212	187 MB

## B Architecture Validation

The two ablations below support the method-design choices used in Section 2. Both target the Huber-TV bw impulse + Gaussian zero-shot mixed-noise setting (§3.3) and train on the two corresponding single-noise STL10 source training sets; only the head or backbone stage selection varies. The first tests whether the denoiser-calibrated slot readout adds value over a plain conditioned MLP head. The second tests whether HyperDn should read only shallow low-level ConvNeXtV2 stages or also include deeper semantic ones. These are architecture checks rather than independent experiments.

### B.1 Ablation: Prediction Head Design

The head ablation compares HyperDn against two alternatives with identical image, data-term, prior, and metadata embeddings: a plain conditioned MLP that treats all padded output slots homogeneously, and a slot-aware affine variant that adds role/scale-dependent affine calibration but omits the bilinear interaction and the denoiser-conditioned multiplicative scale. All variants share the same backbone, training schedule, and seed set (3 seeds); only the head differs.

Table 7: Prediction-head ablation on the zero-shot mixed-noise setting (3 seeds). *Ours* is the denoiser-calibrated slot readout of Eq. (3). “Param. rel. err.” averages  $|\hat{p}_j - p_j^*| / \max(|p_j^*|, 10^{-8})$  over active slots, then over samples; values  $\hat{p}_j, p_j^*$  are in raw hyperparameter space (log-scale slots are decoded by  $10^x$  before computing the error).

Head variant	PSNR $\uparrow$	Gap to oracle (dB) $\downarrow$	Param. rel. err. $\downarrow$
Simple MLP (conditioned, no slot semantics)	$23.72 \pm 0.10$	$0.81 \pm 0.10$	0.255
Slot-aware affine readout	$24.02 \pm 0.14$	$0.50 \pm 0.14$	0.188
Denoiser-calibrated slot readout ( <b>ours</b> )	<b><math>24.29 \pm 0.09</math></b>	<b><math>0.23 \pm 0.09</math></b>	<b>0.160</b>

Role/scale metadata is useful even without the bilinear interaction: the slot-aware affine variant improves over the plain conditioned MLP ( $23.72 \rightarrow 24.02$  dB). The full denoiser-calibrated slot readout adds another 0.27 dB over this intermediate variant and lifts PSNR by 0.57 dB over the plain conditioned MLP ( $23.72 \rightarrow 24.29$ ). It also reduces parameter relative error by 37% ( $0.255 \rightarrow 0.160$ ) and narrows the gap to oracle from 0.81 dB to 0.23 dB. These gains support the combined contribution of slot-semantic conditioning, the bilinear cross-term, and the denoiser-conditioned affine calibration in Eq. (3).

## B.2 Ablation: Backbone Stage Selection

The stage ablation tests whether hyperparameter prediction benefits from deeper semantic features. We compare the default stage choice (0–1) against a single shallow stage (*stage-0 only*) and the full backbone (*stages 0–3*), keeping all other settings identical (same training subset, schedule, head, and seeds).

Table 8: Backbone-stage ablation on the zero-shot mixed-noise setting (3 seeds). *Stages* (0, 1) is our default.

Stage selection	Backbone params	PSNR $\uparrow$	Gap to oracle (dB) $\downarrow$	Param. rel. err. $\downarrow$
Stage 0 only	0.42M	24.06 $\pm$ 0.26	0.46 $\pm$ 0.26	0.174
Stages (0, 1) ( <b>ours</b> )	2.18M	<b>24.29 <math>\pm</math> 0.09</b>	<b>0.23 <math>\pm</math> 0.09</b>	<b>0.160</b>
Full backbone (stages 0–3)	87.69M	23.96 $\pm$ 0.06	0.56 $\pm$ 0.06	0.316

Stages 0 and 1 give the best result: removing stage 1 lowers PSNR by 0.23 dB, while adding the deeper semantic stages 2 and 3 lowers PSNR by 0.33 dB. This pattern is consistent with hyperparameter prediction relying on low-level noise and edge statistics rather than semantic content. Relative parameter error also nearly doubles from 0.160 to 0.316 when deep stages are included, indicating that deeper features hurt this prediction task.

## C Comparison with Classical Methods

The classical baseline comparison is deliberately restricted to the L2-TV + additive-Gaussian axis, where the Monte-Carlo SURE comparator used here is applicable. In that setting, we use the Monte-Carlo SURE procedure of Ramani et al. [2008] as the classical per-image tuning rule for  $\lambda$  under additive Gaussian noise with known or estimable variance. The comparison answers two narrow questions: whether per-image adaptation matters on this classical axis, and whether HyperDn can match or exceed SURE’s quality while being far cheaper per image. For this reason, we do not use SURE for the other settings studied in the main paper.

**Setup.** All methods operate on the same three out-of-distribution test datasets (CBSD68  $321 \times 481$ , Kodak24  $512 \times 768$ , Urban100  $\sim 1024 \times 768$ ) with identical per-image Gaussian noise levels  $\sigma$ :

- **Avg-oracle (fixed  $\bar{p}$ ):** applies the training-set mean oracle hyperparameter vector  $\bar{p}$  to every test image (non-adaptive baseline);
- **SURE** [Ramani et al., 2008]: per-image  $\lambda$  selected by Monte-Carlo SURE minimization, using the ground-truth per-image Gaussian noise level  $\sigma$  from the data-generation process (an upper-bound variant of SURE assuming perfectly known Gaussian variance);
- **HyperDn (ours):** a single forward pass of the source-pretrained HyperDn model;
- **Oracle:** per-image hierarchical grid search (upper bound).

**Results.** Table 9 reports PSNR, gap to oracle, and per-image wall-clock cost across three out-of-distribution test datasets spanning  $321 \times 481$  (CBSD68) to  $\sim 1024 \times 768$  (Urban100). The non-adaptive avg-oracle baseline trails the per-image oracle by 1.19–1.58 dB on average, with large image-to-image variation ( $\pm 1.5$ – $2.0$  dB), confirming that a single global  $\lambda$  is a poor fit.

Against the strongest classical selector in this restricted setting, HyperDn matches or outperforms SURE in quality on every dataset: its gap to oracle is lower in every cell (CBSD68: 0.01 vs. 0.06, Kodak24: 0.27 vs. 0.32, Urban100: 0.02 vs. 0.08 dB). It is also much cheaper per image. SURE selects  $\lambda$  by evaluating a risk estimate over many candidate values; each candidate requires a full TV solve plus an extra solve for Monte-Carlo divergence. Its wall-clock time therefore scales as  $\sim 30\times$  the single-solve reconstruction cost: 2.1 s on CBSD68, 5.7 s on Kodak24, and 11.2 s on Urban100. HyperDn selects  $\lambda$  with one forward pass (14 ms at  $321 \times 481$ , 19 ms at  $512 \times 768$ , 47 ms at  $\sim 1024 \times 768$ ) and then invokes the same TV solver once. Thus the learned predictor replaces SURE’s per-image search with one learned prediction while retaining near-oracle reconstruction quality.

Table 9: Classical comparison on L2-TV Gaussian across three out-of-distribution test datasets. Per-image  $\sigma$  is sampled from the STL10 training range. “Mean gap to oracle” is oracle PSNR minus method PSNR. “Inference” reports only the per-image  $\lambda$ -selection cost; the downstream TV solver is shared and omitted. HyperDn is reported at batch 1 to match SURE’s per-image  $\lambda$  search;  $\pm$  is std over 5 seeds (SURE and Avg-oracle are deterministic).

Dataset	Method	Mean PSNR $\uparrow$	Mean gap to oracle (dB) $\downarrow$	Inference $\downarrow$
CBSD68 ( $321 \times 481$ )	Avg-oracle	25.73	1.19	—
	SURE	26.85	0.06	$\sim 2040$ ms
	<b>HyperDn (ours)</b>	<b><math>26.91 \pm 0.0029</math></b>	<b><math>0.01 \pm 0.0029</math></b>	<b>14 ms</b>
Kodak24 ( $512 \times 768$ )	Avg-oracle	26.44	1.58	—
	SURE	27.70	0.32	$\sim 5530$ ms
	<b>HyperDn (ours)</b>	<b><math>27.75 \pm 0.0030</math></b>	<b><math>0.27 \pm 0.0030</math></b>	<b>19 ms</b>
Urban100 ( $\sim 1024 \times 768$ )	Avg-oracle	24.49	1.37	—
	SURE	25.78	0.08	$\sim 10860$ ms
	<b>HyperDn (ours)</b>	<b><math>25.84 \pm 0.0045</math></b>	<b><math>0.02 \pm 0.0045</math></b>	<b>47 ms</b>